2019

An electromagnetic variable inertance device for seat suspension vibration control

Donghong Ning
Hefei University of Technology, dning@uow.edu.au

Shuaishuai Sun
University of Wollongong, ssun@uow.edu.au

Haiping Du
University of Wollongong, hdu@uow.edu.au

Weihua Li
University of Wollongong, weihuali@uow.edu.au

Nong Zhang
University of Technology Sydney, Hunan University, China, nong.zhang@uts.edu.au

See next page for additional authors

An electromagnetic variable inertance device for seat suspension vibration control

Abstract

This paper designs and builds an electromagnetic variable inertance (VI) device for a heavy duty vehicle seat suspension to reduce the vibration transferred to driver bodies. The conventional semi-active vibration control mainly applies the variable damping (VD) and variable stiffness (VS) devices. The VI device is equivalent to an inerter with the capability to vary its inertance, which is a new semi-active system inspired by the VS device design. The VI device consists of a transmission device, a VD device and two flywheels. By varying the damping of the VD device, the equivalent inertance of the VI device is controllable in real time. The VI device prototype is built with an electromagnetic VD device which is controlled by the duty cycle of the pulse width modulation signal. The test results verify the proposed system model and identify the unknown model parameters. Then, a seat suspension applies the VI device prototype for improving the ride comfort. Based on the system model, an implementable controller is proposed and experimentally validated. The proposed seat suspension system shows excellent performance in a random vibration experiment. Compared with a conventional passive seat suspension, the frequency-weighted root mean square acceleration of the proposed one reduces 35.7%. The VI device has expanded the application of the inerter and the area of the semi-active research; it shows great potential in vibration control.

Disciplines

Engineering | Science and Technology Studies

Publication Details

Ning, D., Sun, S., Du, H., Li, W., Zhang, N., Zheng, M. & Luo, L. (2019). An electromagnetic variable inertance device for seat suspension vibration control. Mechanical Systems and Signal Processing, 133 106259-1-106259-19.

Authors

Donghong Ning, Shuaishuai Sun, Haiping Du, Weihua Li, Nong Zhang, Minyi Zheng, and Liang Luo

An electromagnetic variable inertance device for seat suspension vibration control

Donghong Ning[1, 2], Shuaishuai Sun[2], Haiping Du[2, *], Weihua Li[2], Nong Zhang[1, 3], Minyi Zheng[4], Liang Luo[5]

1. School of Mechanical Engineering, Hefei University of Technology, Hefei, 230000, China

2. Faculty of Engineering and Information Sciences, University of Wollongong, Wollongong, NSW, 2522, Australia.

3. Faculty of Engineering, University of Technology Sydney, Ultimo, NSW, 2007, Australia

4. School of Automotive and Transportation Engineering, Hefei University of Technology, Hefei, 230000, China

5. Automotive Research Institute, Hefei University of Technology, Hefei, 230000, China

*hdu@uow.edu.au

Abstract

This paper designs and builds an electromagnetic variable inertance (VI) device for a heavy duty vehicle seat suspension to reduce the vibration transferred to driver bodies. The conventional semi-active vibration control mainly applies the variable damping (VD) and variable stiffness (VS) devices. The VI device is equivalent to an inerter with the capability to vary its inertance, which is a new semi-active system inspired by the VS device design. The VI device consists of a transmission device, a VD device and two flywheels. By varying the damping of the VD device, the equivalent inertance of the VI device is controllable in real time. The VI device prototype is built with an electromagnetic VD device which is controlled by the duty cycle of the pulse width modulation signal. The test results verify the proposed system model and identify the unknown model parameters. Then, a seat suspension applies the VI device prototype for improving the ride comfort. Based on the system model, an implementable controller is proposed and experimentally validated. The proposed seat suspension system shows excellent performance in a random vibration experiment. Compared with a conventional passive seat suspension, the frequency-weighted root mean square acceleration of the proposed one reduces 35.7%. The VI device has expanded the application of the inerter and the area of the semi-active research; it shows great potential in vibration control.

Key words: Variable inertance; Inerter; Vibration control; Semi-active; Seat suspension; Electromagnetic damper.

1. Introduction

The inerter has attracted many researchers since Smith proposed it [1] at 2002. The inerter has the same unit with the mass element, but it is a two terminals mechanical device similar to the general spring and damper, and its force output is proportional to the relative acceleration between its two terminals. The inerter can benefit the realisation of mechanical systems with arbitrary positive-real impedance and has been applied to vehicle suspensions [2, 3]. Comparing with the traditional passive vehicle suspension, which only has the spring and damper, the inerter-spring-damper system turns to be versatile by given different kinds of configuration. The advantages of inerter are further applied for structural vibration control [4, 5] to provide a potential alternative to the traditional tuned mass damper. The improvement of structures dynamic performance via tuned mass damper and inerter devices is systematically studied [6]. The optimal design of tuned mass damper inerter shows that it can enhance the earthquake resilience of base-isolated structures [7]. The friction and backlash play significant roles in the nonlinear manner of the inerter, which has been experimentally validated [8, 9]; this nonlinearity has an impact on the vehicle suspension performance [10]. The fluid inerter can mitigate the influence of friction in mechanical inerter with helical tubes [11, 12]. In the previous studies about the inerter, researchers have extensively investigated the passive system.

It is well known that the semi-active approach is an economical and effective way for vibration control because it has a better performance than the passive system and requires less energy consumption than an active one. The variable damping (VD) device is the one getting the most attention in terms of the semi-active control studies. The magnetorheological (MR) fluid is popularly applied in the damper design [13-15], which has a quick response to the magnetic field variation with different viscosities, thus, by energising a coil with a variable current to provide a changeable magnetic field, the devices' damping can be controlled. Besides, another kind of smart material, electrorheological (ER) fluid, is also applied in designing VD devices [16, 17]. Electromagnetic VD devices are proposed in [18, 19] which can vary the damping by controlling the resistance in the circuit of an electromagnetic damper. The variable stiffness (VS) device is also widely applied in semi-active control [20]. MR elastomer is a kind of smart material which can continuously vary stiffness [21, 22]; it has shown its excellent performance in vibration control. Another effective way to control a device's equivalent stiffness is to integrate a VD device with springs to form a controllable mechanical network [23]. The semi-active system with inerter is investigated in [24, 25], which shows a significant improvement in vehicle suspension performance compared with the conventional one. A force-tracking approach for a kind of semi-active suspension with the semi-active inerter and the semi-active damper is proposed [26]; the simulation shows that the proposed system can track the active control force much better than the conventional VD one. A novel semi-active inerter is proposed in [27], which designed a controllable-

inertia flywheel to replace the fixed-inertia flywheel. A variable admittance device is introduced with an MR damper, which can control its equivalent inertance [28].

The seat suspension has been widely applied in heavy duty vehicles as these vehicles need to work in severe vibration conditions for a long time. The seat suspension is the most direct way to improve the ride comfort of drivers. Many kinds of seat suspensions have been proposed in the past decades. A passive seat suspension with a negative stiffness property is proposed in [29], which can effectively reduce the low-frequency vibration. In terms of the active seat suspensions, different actuators have been utilised, such as the electromagnetic linear actuator [30], the hydraulic absorber [31], the pneumatic actuator [32] and the rotary motor [33]. The smart materials based solutions are valid for the semi-active seat suspensions [34, 35]. As the seat suspension can be quickly built and tested, it could be an excellent application to validate the novel vibration control technologies.

The VD and VS research has shown the significant advantage of semi-active devices to the passive damper and spring in vibration control systems. Variable inertance (VI) device is a new concept for the semi-active system, which should extend the application of passive inerter. However, the passive inerter is more complicated in structure than its counterparts, namely the damper and spring. The implementation of VI device should be a more significant challenge than VD and VS devices, which is the motivation to conduct this experimental research on the VI device and its application. In this paper, the VI device is proposed, which is a device relative to the inerter as the VD device (respectively, VS device) relative to the damper (respectively, spring); it is an inerter with the capability to vary its equivalent inertance. The conventional inerter requires a transmission device to turn the rotation of a one terminal device, flywheel, to the movement of a two terminals one. By integrating two flywheels and one VD device to form a variable inertia flywheel (VIF), the VI concept can be built. An electromagnetic VD device is used in the VI device prototype to provide a controllable damping force. The VD device and the VI device prototype are both tested to validate the proposed system model and identify the unknown system parameters. Then, the VI device is applied to a seat suspension, and a corresponding controller is designed. The random vibration experiment is implemented to validate the effectiveness of the proposed system, and a conventional passive seat suspension is also tested for comparison.

The rest of the paper is organised as following: Section 2 shows the electromagnetic VI device; In Section 3, the device prototype is tested; the VI seat suspension and its control are shown in Section 4; the experimental evaluations are presented in Section 5; Finally, Section 6 presents the conclusions of this research.

2. The electromagnetic VI device

2.1 VI concept

The effectiveness of inerter in vibration reduction has been validated in many studies. Inerter is a two terminals device similar to its counterparts, the damper and spring; however, it needs a transmission device to connect its two output terminals with a single terminal flywheel. According to the type of transmission device, its output movement can be a linear or rotary one. At the same time, the transmission devices, such as the ball screw and gear reducer, can amplify the rotary speed and torque output of the flywheel; hence, a flywheel with a small moment of inertia is capable of generating a big inertance for the system.

The VD and VS devices have been proposed in papers, and their advantages to the damper and spring with constant parameters are well known. It is easy to think of that the VI device should also have better performance than a constant inerter. As the flywheel's moment of inertia determines the inertance of inerter, an inerter can obtain the variable inertance capability by applying a VIF. In the conventional VS devices design, a VD device connecting with a spring in serial is used to control the device's equivalent stiffness. Inspired by this, a VI device design is shown in Figure 1 where two coaxial flywheels instead of a constant flywheel are mounted on the transmission device, and a rotary VD device is applied to connect the two flywheels. The principle of the VI device design is easy to understand. Assuming that, an ideal VD device is applied, which can vary its damping from zero to infinite. When the damping is zero, the device inertance is determined by flywheel 1 as the flywheel 2 is disconnected. In contrast, when the damping is infinite, the flywheel 1 and 2 are fixedly connected. Therefore, the damping of the VD device can control the device inertance. The two flywheels and the VD device consist of a VIF.

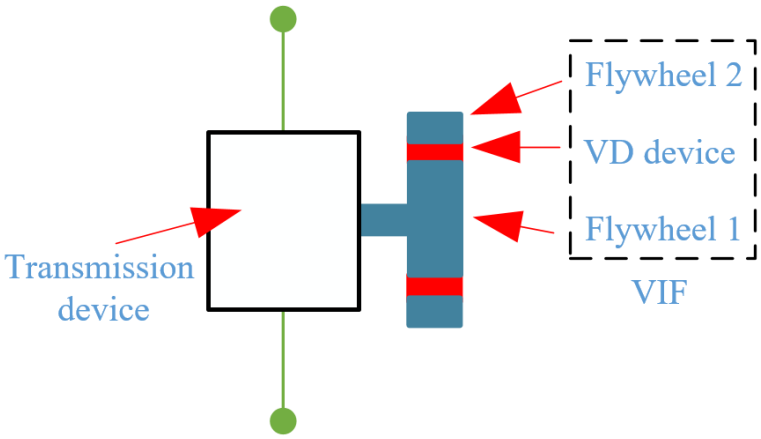

Figure 1. VI device concept.

Figure 2 shows the VI device model, where z_1 and z_2 are displacements of the two terminals, respectively; θ_1 and θ_2 are the rotary angle of flywheel 1 and flywheel 2, respectively; j_1 and j_2 are the moment of inertia of the two flywheels respectively; c_i is the damping of the VD device; the ratio

of the transmission device is r_T, and f_i is the force exerted on the two terminals. Therefore, the VI device model is built as:

$$\theta_1 = r_T(z_1 - z_2) \tag{1}$$

$$f_i = r_T[c_i(\dot{\theta}_1 - \dot{\theta}_2) + j_1\ddot{\theta}_1] \tag{2}$$

$$c_i(\dot{\theta}_1 - \dot{\theta}_2) = j_2\ddot{\theta}_2 \tag{3}$$

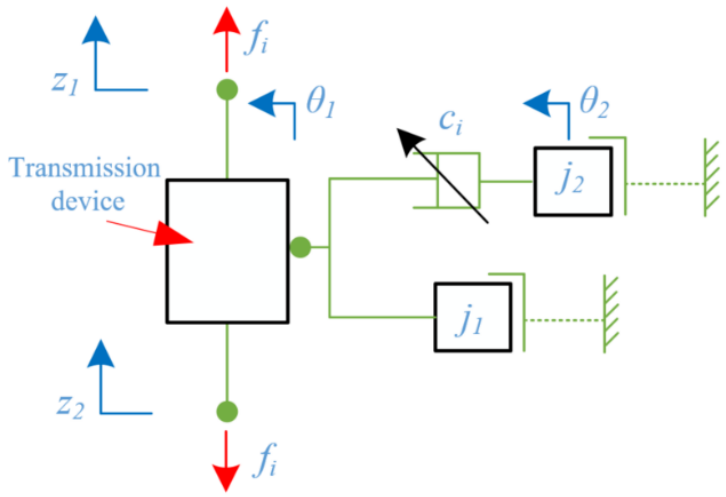

Figure 2. VI device model.

A Laplace domain description can be obtained:

$$\frac{F_i}{(Z_1 - Z_2)s} = j_1 {r_T}^2 s + \frac{j_2 {r_T}^2 s c_i}{j_2 s + c_i} \tag{4}$$

where $F_i(s)$, $Z_1(s)$ and $Z_2(s)$ are the Laplace transforms of $f_i(t)$, $z_1(\mathrm{t})$, and $z_2(\mathrm{t})$.

Hence, the mechanical network admittance of the VI device is:

$$Y = b_1 j\omega + \frac{b_2 j\omega c}{b_2 j\omega + c} = \frac{{b_2}^2 c\omega^2}{c^2 + {b_2}^2\omega^2} + \left(\frac{b_2 c^2}{c^2 + {b_2}^2\omega^2} + b_1\right)\omega j \tag{5}$$

where $b_1 = j_1 {r_T}^2$, $b_2 = j_2 {r_T}^2$, $c = c_i {r_T}^2$. The admittance shows that, with a certain angular frequency ω, the VI device is equivalent to a device in which a variable damper with an equivalent damping $\frac{b_2^2 c\omega^2}{c^2 + b_2^2\omega^2}$ and a variable inerter with an equivalent inertance $b_1 + \frac{b_2 c^2}{c^2 + b_2^2\omega^2}$ are connected in parallel. The equivalent inertance can vary from $b_1$to $b_1 + b_2$, when the damping is controllable.

The VI device admittance further indicates that it is equivalent to a simplified model as shown in Figure 3, where z_{1-3} are the displacement of the upper terminal, connection point and lower terminal, respectively. The device has a constant inertance b_1, and a variable damper connects with an additional inerter in serial.

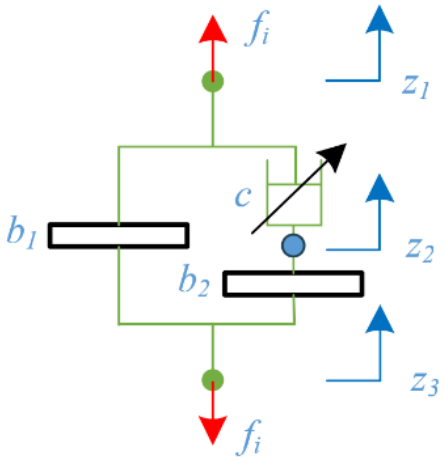

Figure 3. Simplified VI device model.

2.2 Rotary electromagnetic VI device prototype

The electromagnetic VD device has been proposed in [18, 19], which is composed of a motor and a variable resistance circuit; it can vary its damping in real time by controlling the external resistance of the motor. By modifying an electromagnetic VD device, the VI device design is shown in Figure 4. A connector is designed to install the motor stator to the output shaft of the gear reducer. An additional flywheel is fixed with the motor rotor. Hence, the connector and the motor stator constitute the flywheel 1; the motor rotor and the additional flywheel make up the flywheel 2; the variable electromagnetic damping is generated between the motor rotor and stator. This kind of modification can guarantee the free rotation of flywheel 2 as output cables of the VD device are on the motor stator but not on the rotor. The gear reducer drives the flywheel 1 to make the reciprocating motion. The electromagnetic VI device prototype is shown in Figure 5 where a direct current (DC) motor (maxon 370357) is applied.

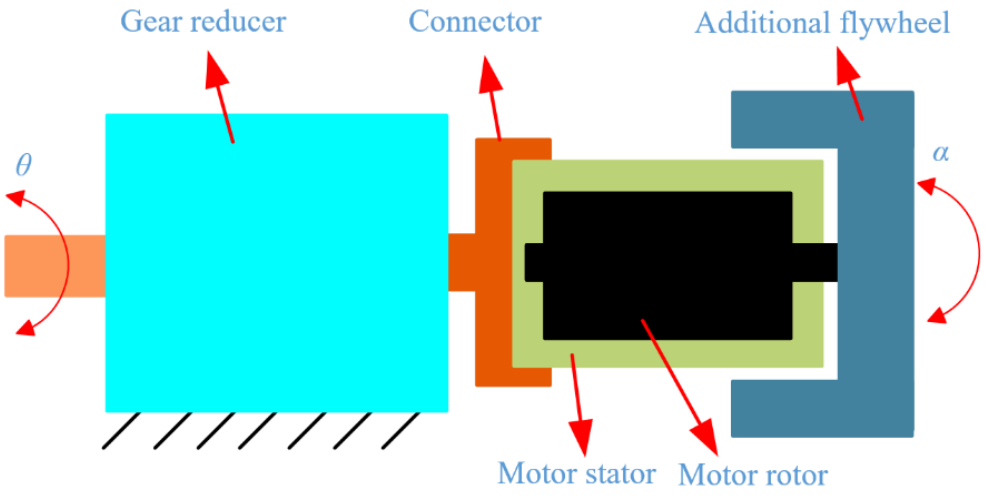

Figure 4. The electromagnetic VI device design.

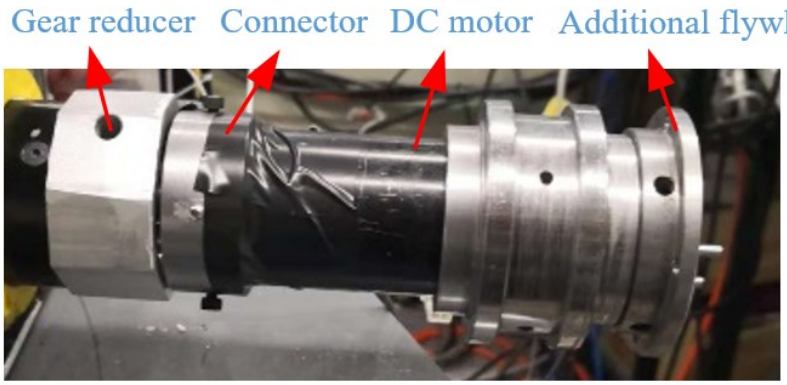

Figure 5. The electromagnetic VI device prototype.

2.3 System circuit

The system circuit of the VI device is shown in Figure 6 which is composed of a DC motor, a variable resistor and a negative impedance converter (NIC); *a, b, c* and *d* are four nodes in the circuit; i is the circuit current. The electromagnetic VD device has a performance bottleneck; the inner resistance of the motor has restricted the maximum damping of the device. Therefore, the NIC, which is proposed in [36] to offset the adverse impact of the inner resistance of the motor, is applied to improve the electromagnetic VD device's mechanical performance.

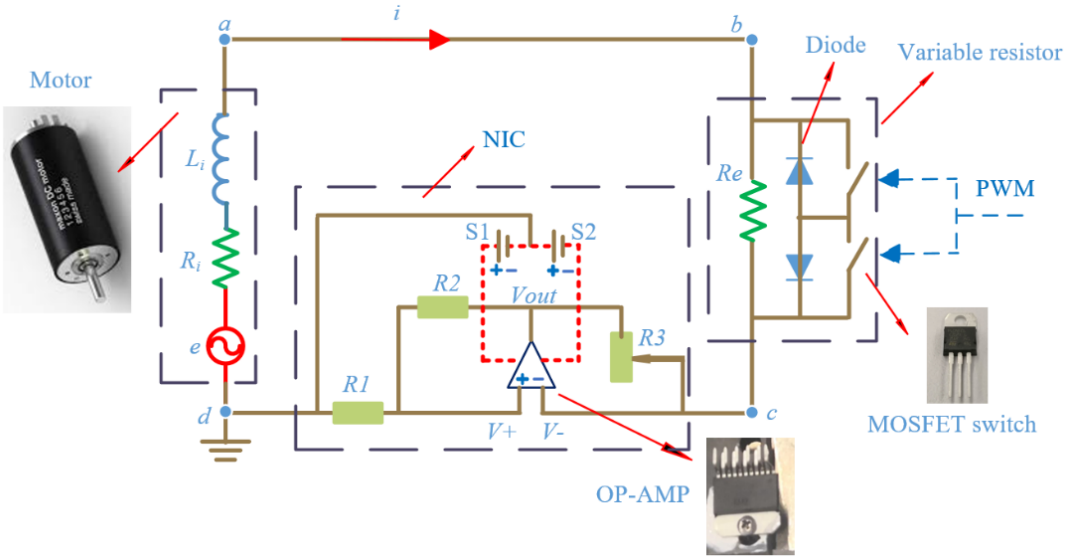

Figure 6. System circuit of the VI device.

The DC motor can be modelled with an inner inductor L_i, an inner resistor R_i and a voltage source e which can generate a voltage in proportion to the motor rotary speed with the motor constant k_i.

The variable resistor consists of a constant resistor R_e=50 Ohm and a bidirectional switch which is composed of two diodes and two metal-oxide-semiconductor field-effect transistor (MOSFET)

switches (N channel, IRF1018EPBF). The two MOSFET switches are controlled by one pulse width modulation (PWM) signal simultaneously. If the two MOSFET switches are off, the equivalent resistance of the variable resistor is R_e; if the switches are on, the ideal resistance will be zero, though the MOSFET switches and diodes may bring resistances. By exerting different duty cycles of the PWM signal, the equivalent resistance of the variable resistor can be controlled. The equivalent resistance is

$$R_E = f(D) \tag{6}$$

where D is the duty cycle of the PWM signal and f is a function which can be identified in experiments.

The NIC consists of an operational amplifier (OP-AMP) (TEXAS INSTRUMENTS, OPA548TG3), three resistors (R_1, R_2 and R_3) and two power supplies (S1 and S2). For an ideal OP-AMP, the voltage across the two input terminals is zero, i.e., $V_+ \approx V_-$; and the current through them can also be assumed to be zero. Thus, the current passes R_1 and R_2 is equal:

$$\frac{V_{out}}{R_1+R_2} = \frac{V_+}{R_1} \tag{7}$$

The current through R_3 is:

$$i = \frac{V_c - V_{out}}{R_3} \tag{8}$$

where V_c is the voltage in node c.

Because $V_c = V_-$, the negative resistance of the NIC can be represented as:

$$R_{NIC} = \frac{V_c}{i} = -\frac{R_1 R_3}{R_2} \tag{9}$$

If $R_1 = R_2$, we can get $R_{NIC} = -R_3$. Therefore, by selecting $R_3 = R_i$, the inner resistor of the motor can be offset. In this paper, $R_1 = R_2 = 1$ M Ohm is applied; $R_3 = R_i = 3.9$ Ohm is found in the datasheet of the motor; S1= S2 = 20 V is used.

In terms of this circuit, two things need to be noted. Firstly, the equivalent resistance function in (6) is related to the motor inner inductor L_i which helps to decrease the ripple of current. We use experiments to identify this function as we mainly study the equivalent state of the circuit. Secondly, by designing a proper motor with a smaller inner resistance R_i and a bigger motor constant k_i (such as applying the three phases brushless motor), the NIC can be omitted from the circuit, then, the system will just require a small power for the PWM signal, which is at milliwatts level. In this paper, the application of the NIC is for the purpose of validation of the VI concept.

2.4 System model

The simplified rotary VI device has been shown in Figure 4 where θ and α are the rotary angles of the gear reducer's input shaft and flywheel 2, respectively; the case of the gear reducer is assumed to be

grounded. The θ is the reciprocating vibration input to the VI device. The rotary angle of flywheel 1 is $\beta = r_g\,\theta$, where r_g is the ratio of the gear reducer.

We can build the model of the VD device firstly. The PWM signal will be exerted on the circuit at a high frequency (5K Hz). Thus the ripple current is existing. The inner inductor L_i (2.83 mH) of the motor is working as a filter to mitigate the ripple current. In terms of the vibration control with the semi-active system, we mainly focus on low frequency vibrations, such as vibrations lower than 5 Hz. As the circuit dynamic is much faster than our focusing frequency, we can just study the equivalent current, voltage and resistance of the circuit. At the same time, as we focus on the low frequency behaviour of the system, the impedance of the inner inductor L_i is very low. Hence, the inductor has little influence on the equivalent system; we ignore the effect of the inductor for simplification [37].

The induced voltage of the VD device is proportional to the relative rotary velocity of its rotor and stator:

$$e = k_i\left(\dot{\beta} - \dot{\alpha}\right) \tag{10}$$

As the NIC has offset the resistance of the motor coil, the circuit current is:

$$i = \frac{e}{f(D)+R_0} \tag{11}$$

where R_0 is the resistance caused by circuit cables and components.

The torque output of the VD device can be defined as:

$$T_m = -k_i i \tag{12}$$

Thus, the damping of the electromagnetic VD device is:

$$c_m = -\frac{T_m}{\dot{\beta}-\dot{\alpha}} = \frac{{k_i}^2}{f(D)+R_0} \tag{13}$$

It shows that the damping of the VD device can be controlled by the duty cycle of the PWM signal.

The torque of the rotary VI device includes two parts, T_1 and T_2 which are generated by the constant flywheel 1 and the electromagnetic VD device, respectively. T_2 is actually the interacted torque between the two flywheels, and is controllable.

T_1 can be defined as:

$$T_1 = r_g\ddot{\beta}J_1 = {r_g}^2 J_1\,\ddot{\theta} \tag{14}$$

where J_1 is the moment of inertia of the flywheel 1.

The dynamic equation of the flywheel 2 is:

$$c_m\left(\dot{\beta}-\dot{\alpha}\right)=J_2\ddot{\alpha} \tag{15}$$

where J_2 is the moment of inertia of the flywheel 2.

The second part of the torque output is:

$$T_2=r_g c_m\left(\dot{\beta}-\dot{\alpha}\right) \tag{16}$$

Therefore, the system model of the VI device is:

$$T=T_1+T_2 \tag{17}$$

3. Prototype test

In this section, tests are implemented to validate the system model and identify the unknown parameters.

3.1 Test system

Experiments are designed to test the VD and VI device prototypes, as shown in Figure 7. The devices are connected to a servo motor (Panasonic, 400 W) by a coupling without a gear reducer. Hence, the transmission ratio of the servo motor and devices is one, which means that the ratio of gear reducer in the proposed model can be taken as one. For the VD device test, the state of the motor is grounded, and the servo motor drives the rotor. For the VI device test, the flywheel 1 of the VIF, the connector, is fixed with the servo motor, and the additional flywheel can rotate freely. A controller (NI CompactRio 9074) is used to control the servo motor rotation. At the same time, the controller can acquire the actual rotation angle from the encoder on servo motor, the servo motor's torque output from its driver, and the currents and voltages in the circuit.

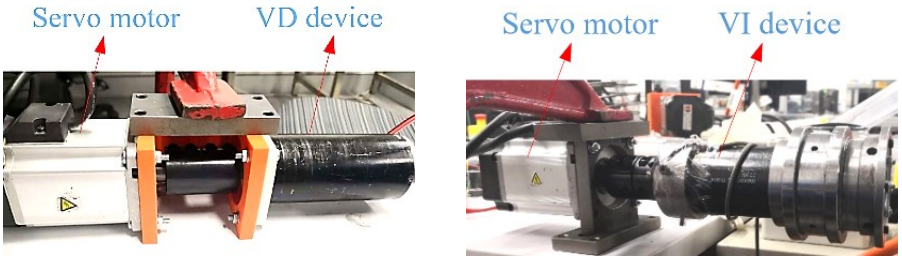

(a) (b)

Figure 7. Prototype test. (a) VD device. (b) VI device.

3.2 VD device test

As the VI device prototype is built based on the VD device, the VD device model is required to be validated first. An experiment for obtaining the function of the equivalent resistance is designed. The nodes *c* and *d* in the circuit are shorted for getting rid of the influence of the NIC. The servo motor is controlled to rotate at certain speeds, and the circuit is exerted with different duty cycles of the PWM

signal; the circuit current and the voltage at the two terminals of the variable resistor are recorded. Then, the equivalent resistances are acquired by using the voltage to divide the current. In Figure 8, the equivalent resistances are almost coincident with a certain PWM duty cycle and different rotation speeds. It indicates that the PWM signal can stably control the equivalent resistance. Hence, a polynomial is selected to fit the experimental results:

$$R_E = f(D) = -26.37D^3 + 73.44D^2 - 95.43D + 49.08 \quad (18)$$

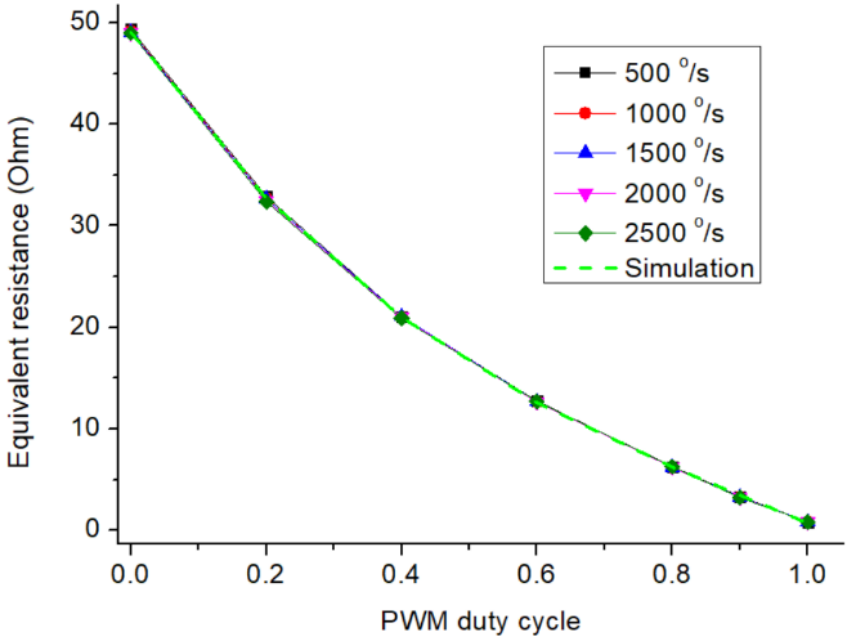

Figure 8. Equivalent resistance.

With the circuit in Figure 6, the VD device is further tested. The servo motor is controlled to make a sinusoidal movement with 2 Hz frequency and 200° amplitude. As the torque of the VD device is proportional to the circuit current *i*, the results in Figure 9 indicate that the system damping is increasing with the increase of the PWM duty cycle. The motor constant $k_i = 0.242$ Nm/A is found in the datasheet of the motor. By inputting the measured rotary velocity into $\dot{\omega} - \dot{\alpha}$ of (8) and (11), $R_0 =$ 2.3 Ohm is identified based on the test result. The simulation results can basically fit the experimental one, which can verify the VD device model. It needs to be noted that the device current is saturated around 2 A which is determined by the NIC as the OP-AMP in it has a limited capability. Based on this test, we can know that the damping of the VD device c_m can be varied from 0.00114 Nm/(rad/s) to 0.01865 Nm/(rad/s), and the maximum torque output T_{max} is 0.48 Nm.

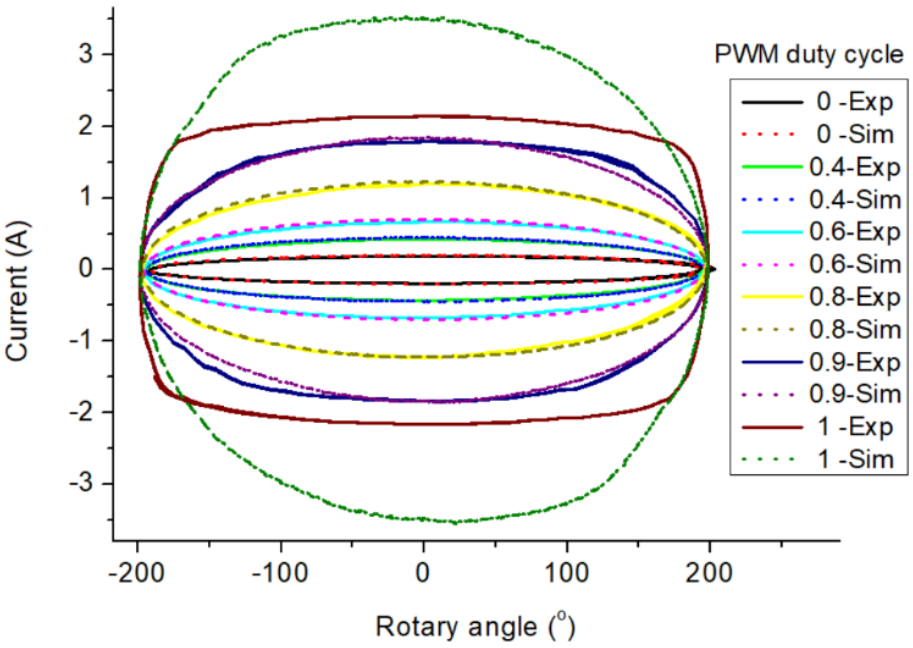

Figure 9. The current-rotary angle of the VD device.

The NIC performance with different PWM duty cycles is shown in Figure 10 where the voltages between nodes c and d are measured, and the desired voltage is defined as $V_d = -iR_i$. When the PWM duty cycle is zero, the NIC can accurately provide the desired voltage compensation. When the PWM duty cycle is 0.8, the system dynamic caused by the MOSFET switches will introduce high frequency noises, however, the desired voltage can basically match the equivalent voltage of the measured one. The test has verified the effectiveness of the NIC.

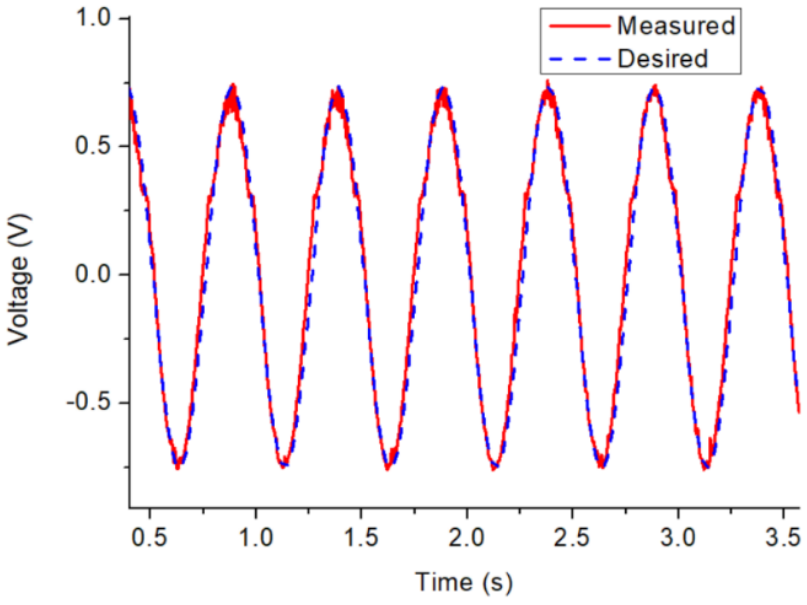

(a)

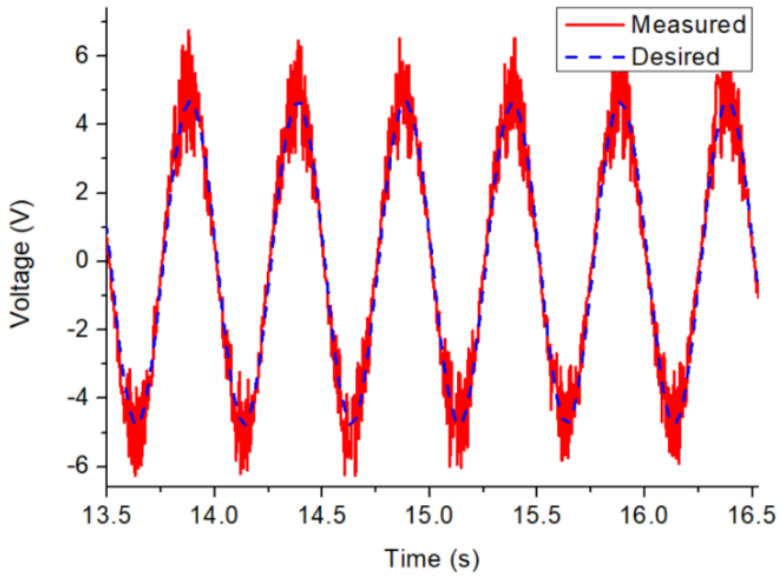

(b)

Figure 10. NIC performance with different PWM duty cycles. (a) Duty cycle 0. (b) Duty cycle 0.8.

3.3 VI device test

In the VI device test, the servo motor does a sinusoidal rotation with 2 Hz frequency and 200° amplitude. The second part of the VI device model can be also written as:

$$T_2 = -k_i i r_g \tag{19}$$

where $r_g = 1$ in this test. Hence, the circuit current is proportional with the second part torque.

The induced current with respect to the rotary angle of the VI device is shown in Figure 11. According to (19), the electromagnetic torque of the VI device is obtained, as shown in Figure 12, where the slope of the graphic indicates the equivalent stiffness of the system. As the electromagnetic torque-rotary angle graphic has a negative slope, the VI device shows a negative stiffness behaviour. The results show that the torque output of the flywheel 2 and the VD device can be controlled, and the system equivalent stiffness can be varied by exerting different duty cycles of PWM signal. The inerter can generate a negative stiffness behaviour in the sinusoidal movement; with a specific frequency, the magnitude of the negative stiffness is increasing with the inertance of the device. Hence, the results imply that, with the increase of the PWM duty cycle, the equivalent inertance is increasing.

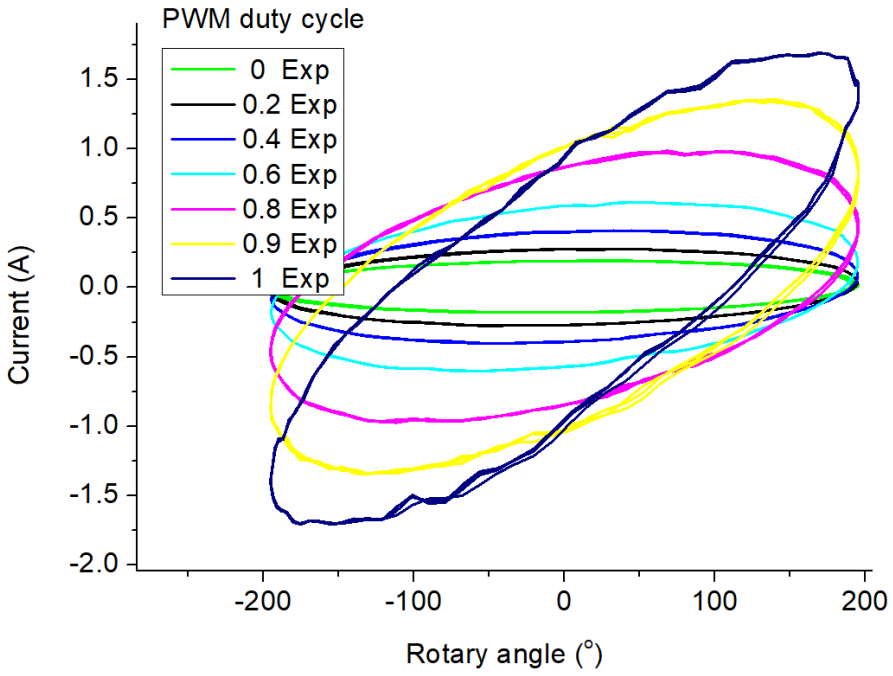

Figure 11. The current-rotary angle of the VI device.

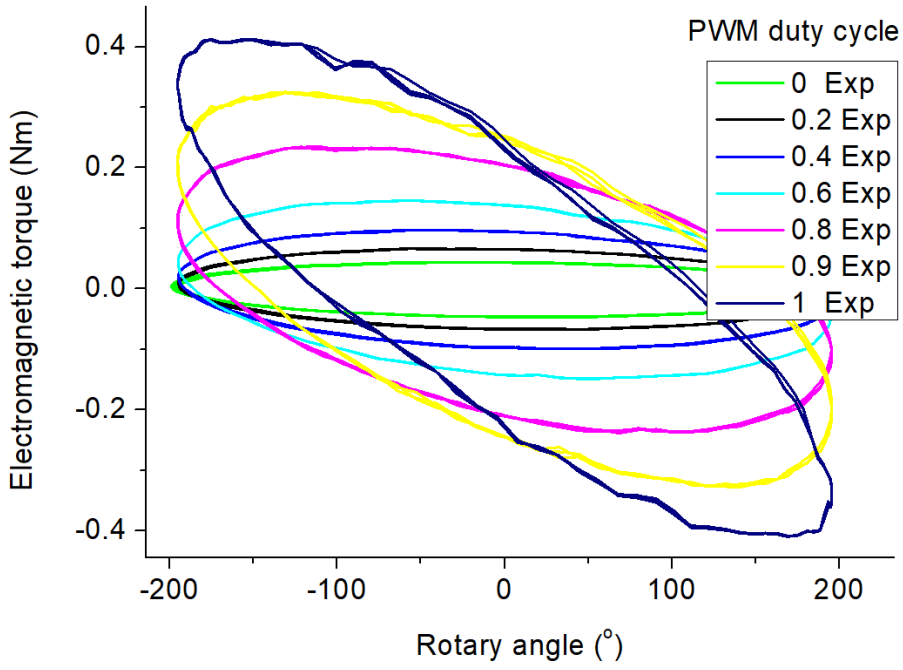

Figure 12. The electromagnetic torque-rotary angle of the VI device.

The simulation applies the proposed model. Based on the test results, the moment of inertia of the flywheel 2 is identified as $J_2 = 770 * 10^{-6}$ Kgm^2. In Figure 13, the simulation results can basically match with the experiment. Hence, the proposed model can be applied to depict the system dynamics.

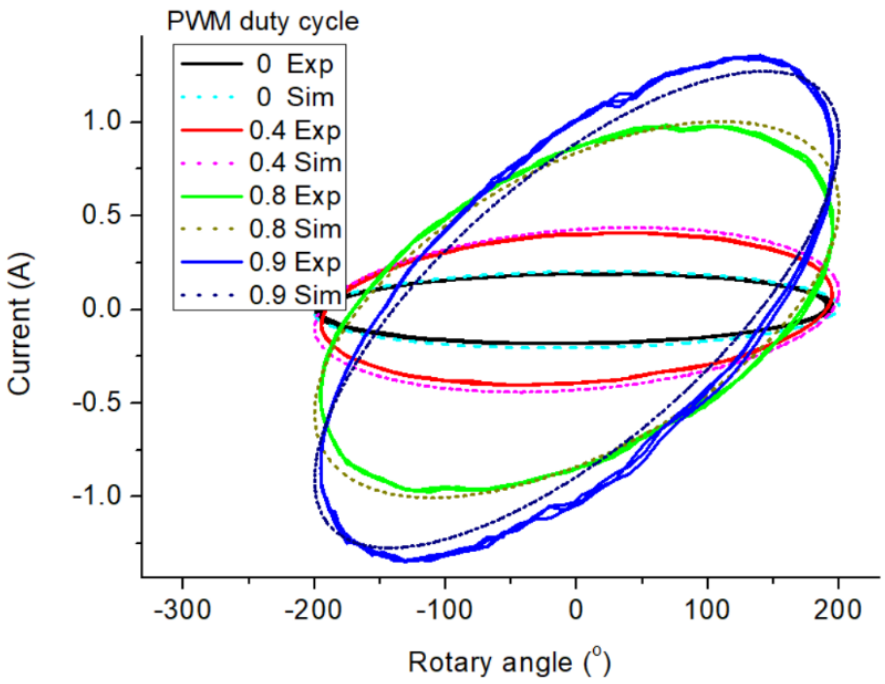

Figure 13. VI device model verification.

The measured torque output from the servo motor can be simplified as:

$$T_m = {r_g}^2(J_1 + J_m)\ddot{\theta} + f_0 \text{sign}(\dot{\theta}) + T_2 \tag{20}$$

where J_m is the moment of inertia of the servo motor, θ is the rotary angle of the servo motor, f_0 is the friction parameter, and T_2 can be obtained based on (19).

Thus, the torque without T_2 can be obtained:

$$T_r = {r_g}^2(J_1 + J_m)\ddot{\theta} + f_0 \text{sign}(\dot{\theta}) = T_m - T_2 \tag{21}$$

The VI device is controlled by PWM duty cycles. Figure 14 shows that, with different PWM duty cycles, the results of T_r are almost overlapped, which means that T_r is independent with the device control. Based on the test results, $J_1 + J_m = 470 * 10^{-6}$ Kgm^2 and $f_0 = 0.1$ Nm are identified. Hence, the simplified model in (20) and (21) is validated.

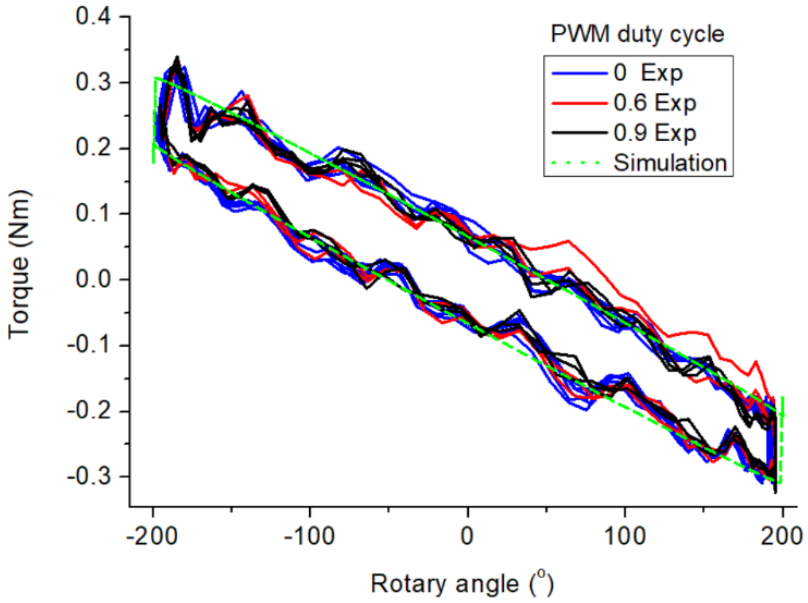

Figure 14. Torque output without T_r.

By removing the device prototype, the torque output of the servo motor without load is also tested with the same sinusoidal rotation. The toque model of the motor can be built as:

$$T_n = {r_g}^2(J_m)\ddot{\theta} + f_0 \text{sign}(\dot{\theta}) \tag{22}$$

Hence, based on the test result, the moment of inertia of the servo motor $J_m = 100 * 10^{-6}$ Kgm^2 can be identified. Figure 15 shows that the simplified model can be applied to the system. Combining (21), we can get the moment of inertia of flywheel 1 $J_1 = 370 * 10^{-6}$ Kgm^2.

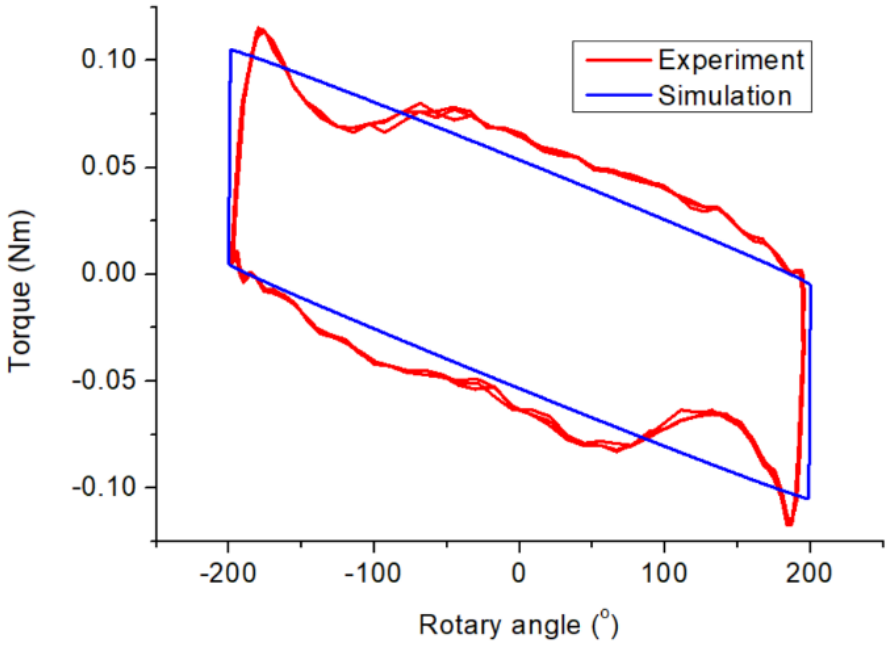

Figure 15. Torque output of servo motor without load.

4. The VI seat suspension vibration control

In this section, a seat suspension prototype with a VI device is introduced, and an implementable controller is proposed to validate the effectiveness.

4.1 Seat suspension with a VI device

By modifying a conventional passive seat suspension (GARPEN GSSC7), the proposed rotary VI device is installed as shown in Figure 16. The original damper in the seat suspension is removed, and the VI device is mounted on the centre of the scissors structure. The transmission ratio of the applied gear reducer is 40.

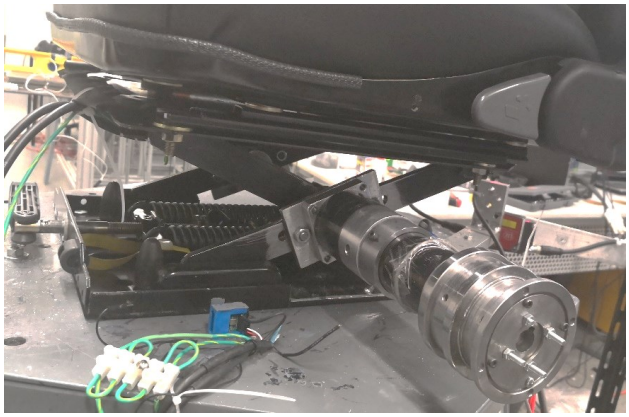

Figure 16. Seat suspension prototype with a VI device.

The structure of the seat suspension is shown in Figure 17 where the scissors structure can transform the vertical movement of the seat suspension to a rotary one. The rotary angle of the scissors structure can be written as:

$$\theta_0 + \theta = 2\text{asin}(\frac{h_0+h}{l}) \tag{23}$$

where $h_0 = 0.11$ m is the initial suspension height; $\theta_0 = 0.786$ rad is the initial angle; h is the relative movement of suspension; $l = 0.287$ m is the length of the bar.

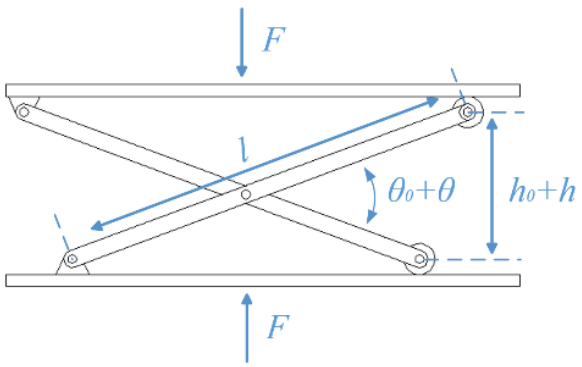

Figure 17. Structure of the seat suspension.

Hence, the rotary rate of the scissors structure is obtained as:

$$\dot{\theta} = \frac{2\dot{h}}{\sqrt{l^2-(h_0+h)^2}} \tag{24}$$

We assume that h can move within ± 0.025 m, it is easy to find that:

$$r_s = \frac{2}{\sqrt{l^2-(h_0+h)^2}} \approx \frac{2}{\sqrt{l^2-{h_0}^2}} \approx 7.5448 \tag{25}$$

Therefore, the transmission ratio between the linear and rotary movement can be linearised as $\theta \approx r_s h$, $\dot{\theta} \approx r_s \dot{h}$ and $\ddot{\theta} \approx r_s \ddot{h}$.

As the VI device is installed on the scissors structure, the rotation of its gear reducer is shown in Figure 18 where the rotary angle of the input shaft is $\theta/2$, and the case of the gear reducer rotates $-\theta/2$. Hence, the rotary angle of the flywheel 1 is $\theta(r_g - \frac{1}{2})$; the actual transmission ratio of the VI device in the system is $r_g - \frac{1}{2}$.

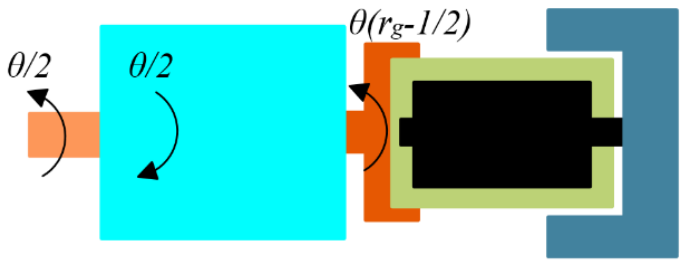

Figure 18. The VI device rotation in the seat suspension.

In section 3, we have identified parameters of the rotary VI device with a transmission ratio of one; then, we can get the equivalent inertance and damping of the VI device in terms of the seat suspension.

$$b_1 = (r_s(r_g - \tfrac{1}{2}))^2 J_1 \approx 32.86 \text{ Kg} \tag{26}$$

$$b_2 = (r_s(r_g - \tfrac{1}{2}))^2 J_2 \approx 68.39 \text{ Kg} \tag{27}$$

$$c = (r_s(r_g - \tfrac{1}{2}))^2 c_m \in (101.25 \text{ Ns/m}, 1656.40 \text{ Ns/m}) \tag{28}$$

Hence, if the ideal damping is applied, the equivalent inertance of the seat suspension can vary from 32.86 Kg to 101.25 Kg.

The maximum force output from the controllable part of the VI device is:

$$F_{max} = r_s \left(r_g - \frac{1}{2}\right) T_{max} \approx 143.05\text{N} \tag{29}$$

4.2 Seat suspension analysis

For analysing the vibration control capability of the VI seat suspension, a linearised model is shown in Figure 19 where k is the seat suspension stiffness, c_1 is the equivalent damping caused by frictions, and b_1, b_2 and c_2 are the inertance of flywheel 1, the inertance of flywheel 2 and the variable damping of the VI device, respectively. m is the suspended mass. z_s, z_c and z_v are the displacement of the seat, the connection point and the cabin floor, respectively. People generally study the low-frequency vibration of the seat suspension, where the nonlinear part of damping and stiffness is trivial; hence, we only consider the linear model in this paper for simplification.

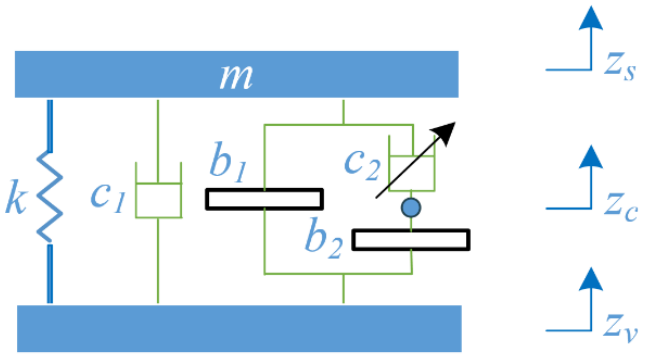

Figure 19. Seat suspension model.

The dynamics of the seat suspension can be built as:

$$m\ddot{z}_s = -k(z_s - z_v) - c_1(\dot{z}_s - \dot{z}_v) - b_1(\ddot{z}_s - \ddot{z}_v) - c_2(\dot{z}_s - \dot{z}_c) \tag{30}$$

$$c_2(\dot{z}_s - \dot{z}_c) = b_2(\ddot{z}_c - \ddot{z}_v) \tag{31}$$

Therefore, the Laplace domain description of the vibration transmissibility of the seat suspension from the cabin floor to the seat surface is:

$$\frac{Z_s}{Z_v} = \frac{k+c_1 s+b_1 s^2+\frac{c_2 b_2 s^2}{b_2 s+c_2}}{ms^2+k+c_1 s+b_1 s^2+\frac{c_2 b_2 s^2}{b_2 s+c_2}} \tag{32}$$

where $Z_s(s)$ and $Z_v(s)$ are the Laplace transforms of $z_s(t)$ and $z_v(\mathrm{t})$.

By evaluating the Laplace transform along the $j\omega$ axis in the complex s plane, the vibration transmissibility is:

$$\frac{Z_s}{Z_v} = \frac{j\left(kb_2\omega+c_1c_2\omega-b_1b_2\omega^3\right)+\left(kc_2-c_1b_2\omega^2-b_1c_2\omega^2-c_2b_2\omega^2\right)}{j(-mb_2\omega^3+kb_2\omega+c_1c_2\omega-b_1b_2\omega^3)+(-mc_2\omega^2+kc_2-c_1b_2\omega^2-b_1c_2\omega^2-c_2b_2\omega^2)} \tag{33}$$

The vibration transmissibility of the seat suspension $|\frac{Z_s}{Z_v}|$ with four different kinds of configurations, which are shown in Table 1, are presented in Figure 20, where m = 75 Kg and k = 6600 N/m. In cases

1 and 2, the VI device is not applied, and only the damping is changed. It can be observed that, by varying the damping, the resonance peak of transmissibility can be suppressed; but it keeps higher than one, which means that the vibration from the cabin floor is still amplified. In case 4, the damping in the VI device is selected as a relatively high value, which means a high equivalent inertance is applied; the vibration transmissibility around the initial resonance frequency is lower than one which indicates that the vibration has been isolated. Though a small peak is retained around 1 Hz for case 4, it is hard to appear in practice as the existing of the friction. An enormous magnitude of vibration is required to conquer the friction, then the suspension can have relative movements at a low-frequency vibration (lower than 1 Hz); the vibration transmissibility will keep around one in practice.

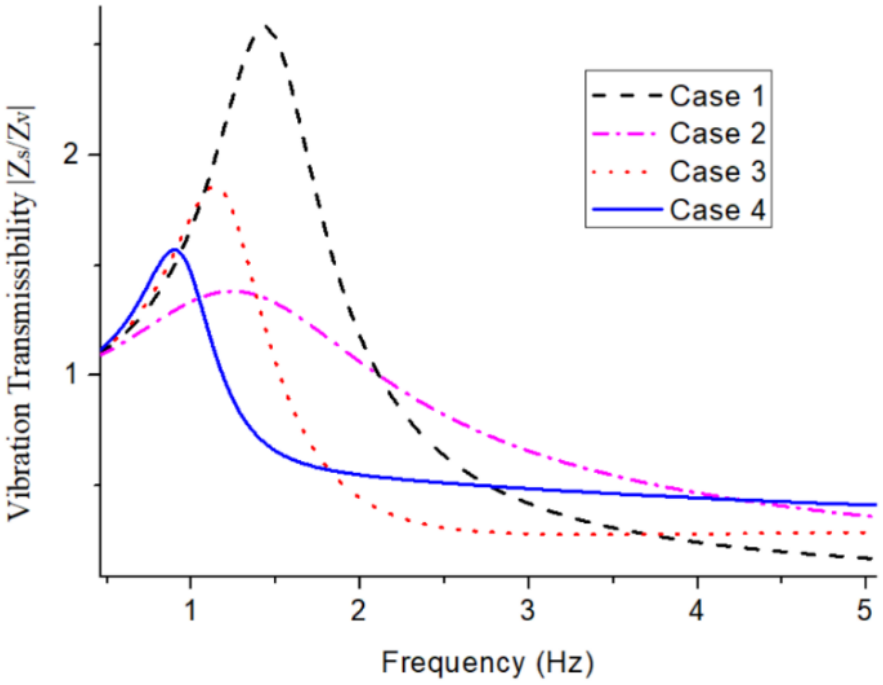

Figure 20. Vibration transmissibility.

Table 1. Seat suspension configurations.

	c_1 (Ns/m)	c_2 (Ns/m)	b_1 (Kg)	b_2 (Kg)
Case 1	300	-	-	-
Case 2	800	-	-	-
Case 3	300	101	32	68
Case 4	300	800	32	68

Compared to the conventional VD seat suspension, the proposed VI seat suspension has an advantage in vibration control around the resonance vibration. Generally, the highest vibration magnitude of the heavy duty vehicle seat is in the range of 2 to 4 Hz [38], thus, based on the simulation, the VI seat suspension will have a better performance than the conventional semi-active seat suspension in

improving the ride comfort. The VI seat suspension can be further optimised, such as decreasing b_1, namely, the inertance of the flywheel 1.

4.3 Controller design

In the semi-active control, an effective strategy is to design an active controller firstly; then applying the semi-active device to track the desired active force. In this paper, the VI device is used to simulate the desired active force of an active H_∞ controller.

The current in the circuit can be easily measured, which can indicate the torque output of the VI device's controllable part. Hence, the system model (30) can be rewritten as:

$$m\ddot{z_s} = -k(z_s - z_v) - c_1(\dot{z_s} - \dot{z_v}) - b_1(\ddot{z_s} - \ddot{z_v}) + u \tag{34}$$

where $u = -k_i i(r_g - \frac{1}{2})r_s$.

By selecting the state variables as $x_1 = z_s - z_v$, $x_2 = \dot{z_s}$ and the disturbances as $d_1 = -\dot{z_v}$, $d_2 = c_1\dot{z_v} + b_1\ddot{z_v}$, the suspension model can be written as a state space form:

$$\dot{\mathbf{X}} = \mathbf{AX} + \mathbf{B_1}\boldsymbol{\omega} + \mathbf{B_2}u \tag{35}$$

where $\mathbf{X} = [x_1\ x_2]^{\mathrm{T}}$, $\mathbf{A} = \begin{bmatrix} 0 & 1 \\ -\frac{k}{m+b_1} & -\frac{c_1}{m+b_1} \end{bmatrix}$, $\mathbf{B_1} = \begin{bmatrix} 1 & 0 \\ 0 & \frac{1}{m+b_1} \end{bmatrix}$, $\boldsymbol{\omega} = [d_1\ d_2]^{\mathrm{T}}$, $\mathbf{B_2} = [0\ \frac{1}{m+b_1}]^{\mathrm{T}}$.

The acceleration of the driver body is applied to evaluate the ride comfort. Thus, the controlled output is defined as:

$$z = \mathbf{C_1X} + \mathbf{D_{11}}\boldsymbol{\omega} + \mathrm{D}_{12}u \tag{36}$$

where $\mathbf{C_1} = \begin{bmatrix} -\frac{k}{m+b_1} & -\frac{c_1}{m+b_1} \end{bmatrix}$, $\mathbf{D_{11}} = \begin{bmatrix} 0 & \frac{1}{m+b_1} \end{bmatrix}$, $\mathrm{D}_{12} = \frac{1}{m+b_1}$.

The H_∞ controller is employed for this system as the it is highly robust to uncertainties and is easy to implement.

Hence, the state feedback H_∞ controller is designed as:

$$u = \mathbf{KX} \tag{37}$$

where $\mathbf{K}$ is the feedback gain to be designed.

The solution of $\mathbf{K}$ is not involved in this paper as it has been presented many times in literature [19].

When the flywheels 1 and 2 in the VI device have a relative rotation β_r, a voltage is induced, which is:

$$e = k_i\dot{\beta}_r = V_{ad} + iR_i \tag{38}$$

where V_{ad} is the measured voltage of the motor's two output terminals.

Hence, a desired damping between the two flywheels is:

$$c_d = -\frac{u}{\dot{\beta}_r(r_g-\frac{1}{2})r_s} = \frac{{k_i}^2 i}{V_{ad}+iR_i} \tag{39}$$

The practical damping of the VD device should be a positive one, and is limited between:

$$c_{min} = \frac{{k_i}^2}{f(0)+R_0} \tag{40}$$

$$c_{max} = \frac{{k_i}^2}{f(1)+R_0} \tag{41}$$

where c_{min} is the minimum damping when the PWM duty cycle is zero and c_{max} is the maximum damping when the PWM duty cycle is one.

Therefore, an implementable control method is proposed:

If $c_d < c_{min}$, the PWM duty cycle is set as 0. If $c_d > c_{max}$, the PWM duty cycle should be 1. If $c_{min} \le c_d \le c_{max}$, a PWM duty cycle D_t can obtained by solving:

$$f(D_t) = \frac{V_{ad}+iR_i}{i} - R_0 \tag{42}$$

Therefore, the controller implementation is shown as in Figure 21.

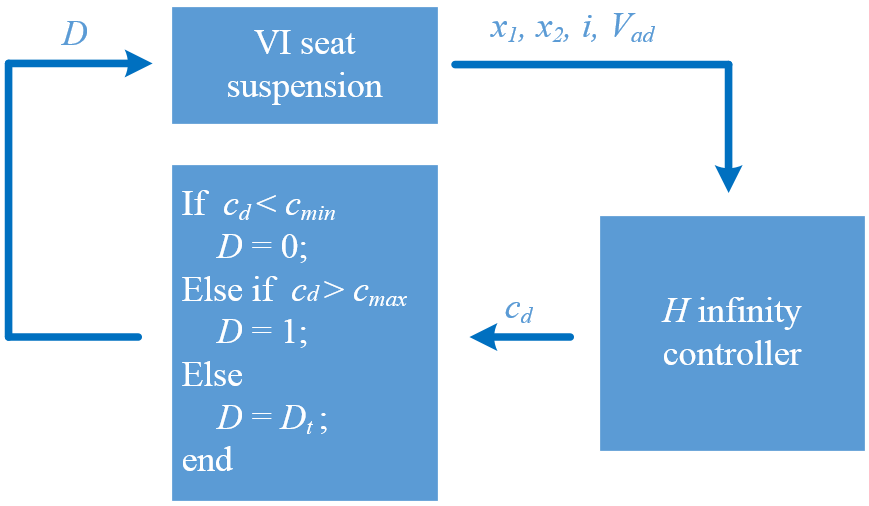

Figure 21. Controller implementation.

5. Vibration experiments

5.1 Experiment setup

The vibration control experiments are implemented with a six-degree of freedom (6-DOF) vibration platform as shown in Figure 22. A 65 Kg sandbag is applied to simulate the driver's weight. A controller (NI CompactRio 9074) is used to acquire the sensors data which includes the motor current, seat acceleration, vibration acceleration, seat displacement and suspension deflection; based on the feedback, the proposed control algorithm runs in the controller, and the system circuit is controlled. A conventional passive seat suspension (GARPEN GSSC7) is also involved in this experiment for comparison.

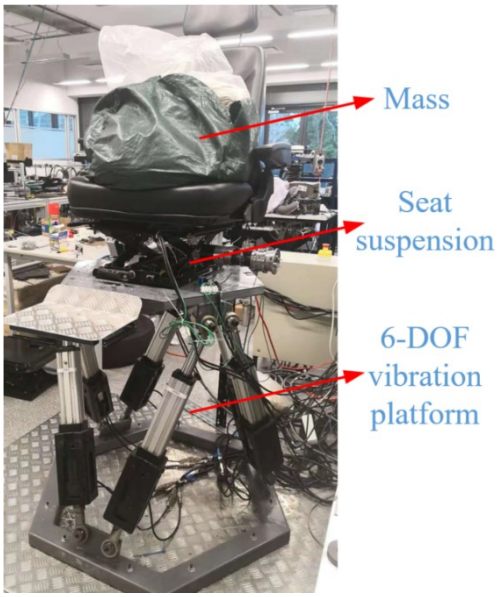

Figure 22. Vibration experiment rig.

5.2 Random vibration

In the random vibration, the desired control force is shown in Figure 23; based on it, the desired current through the system for active control is obtained, which is

$$i_d = -\frac{u}{k_i(r_g - \frac{1}{2})r_s} \tag{43}$$

In Figure 24, the desired current and the measured current is presented. The measured current seems have not tracked the desired one well, but it is a common phenomenon for semi-active systems. If there is an additional active power to supply the desired current totally, the system can have its best performance. However, the additional active power does not exist in a semi-active system. The applied motor in the vibration induces the measured current. The proposed system can control the induced current to track a part of the desired current, and hence, generate a beneficial force to improve the seat suspension's performance in vibration isolation. Other advanced controllers, such as the fuzzy sliding mode controller [39] and neuro-fuzzy training algorithms [40, 41], which have proved their

effectiveness in variable damping systems, are available to improve the current tracking capability of the variable inertance system.

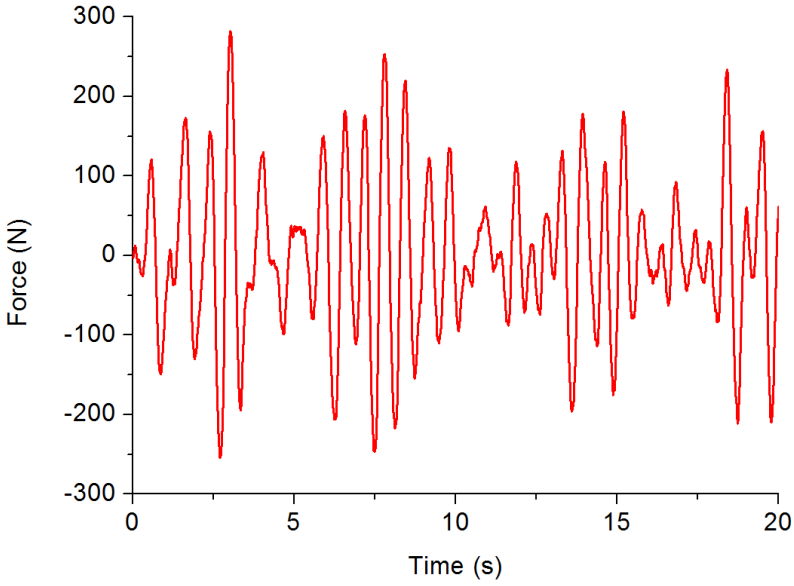

Figure 23. Desired control force.

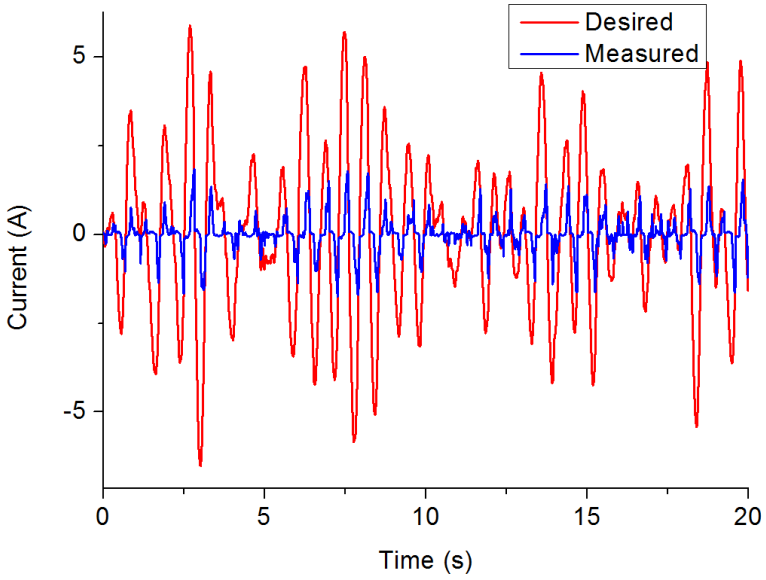

(a)

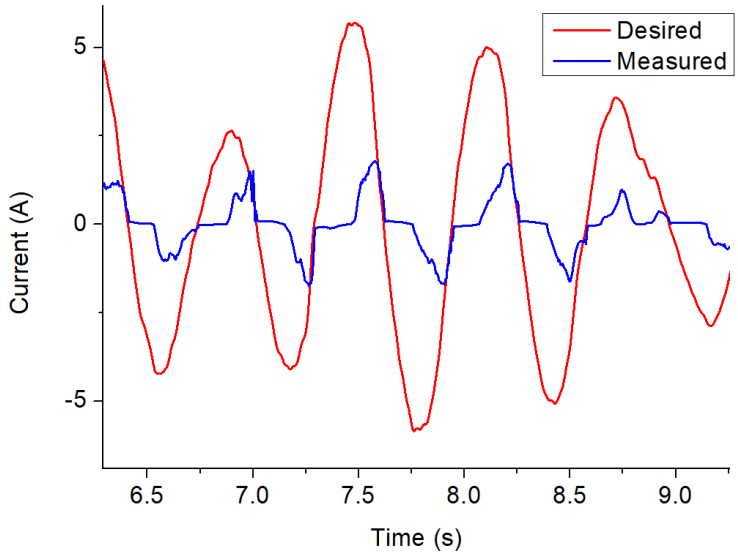

(b)

Figure 24. The desired and measured current. (a) Entire experiment. (b) Zoom in.

The seat accelerations comparison of the proposed system and the conventional passive one is shown in Figure 25 where the high magnitude peak of the acceleration is successfully reduced. The frequency analysis in Figure 26 indicates that, both seat suspensions can isolate vibration in frequencies higher than 3.5 Hz. With the resonance vibration around 1.6 Hz, the passive one amplifies the vibration, while the VI seat suspension can isolate the vibration. Based on ISO 2631-1 [42], the frequency weighted-root mean square (FW-RMS) acceleration and the fourth power vibration dose value (VDV) are obtained to evaluate the seat suspensions' performance. In Figure 27, the reduction of the FW-RMS indicates the improvement of ride comfort, and the VDV values show that the VI seat suspension has a superior performance in the shock vibration.

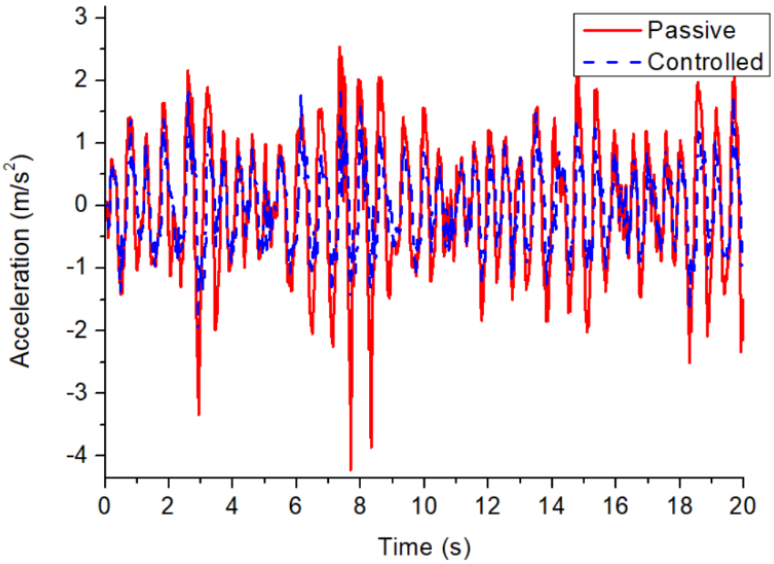

Figure 25. Seat acceleration in the time domain.

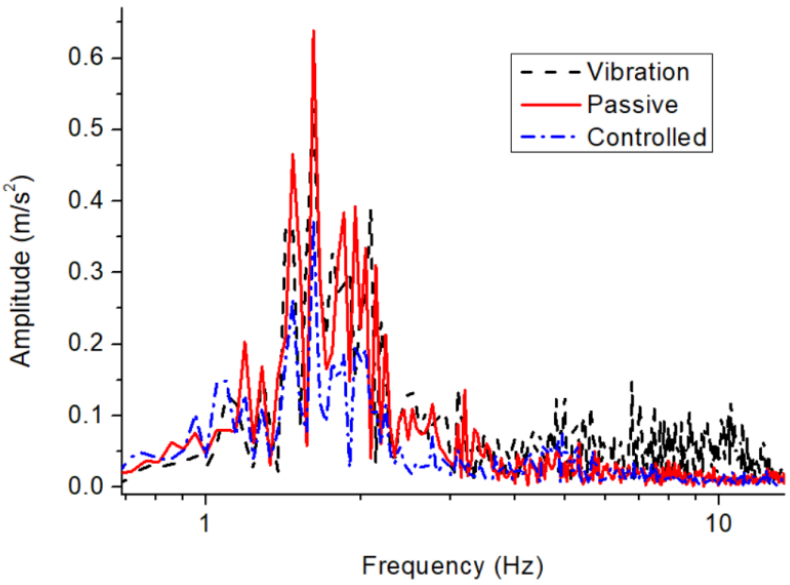

(a)

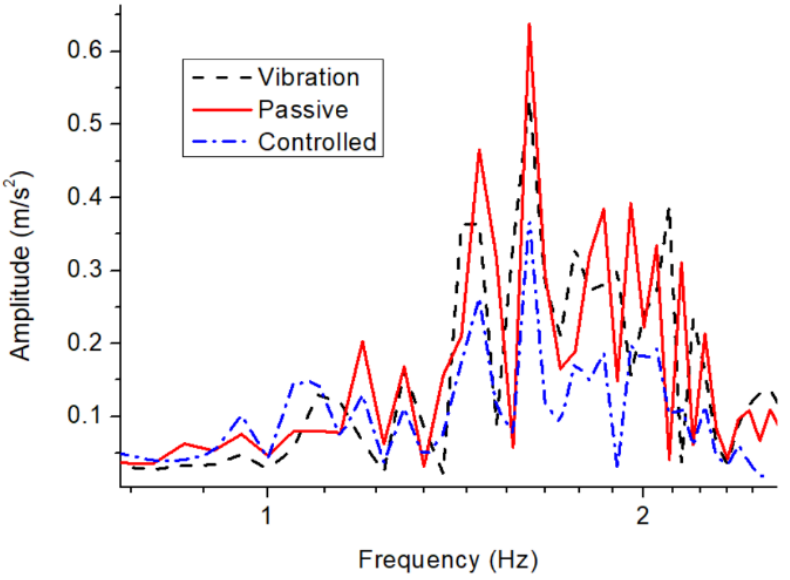

(b)

Figure 26. Acceleration in the frequency domain. (a) Entire experiment. (b) Zoom in.

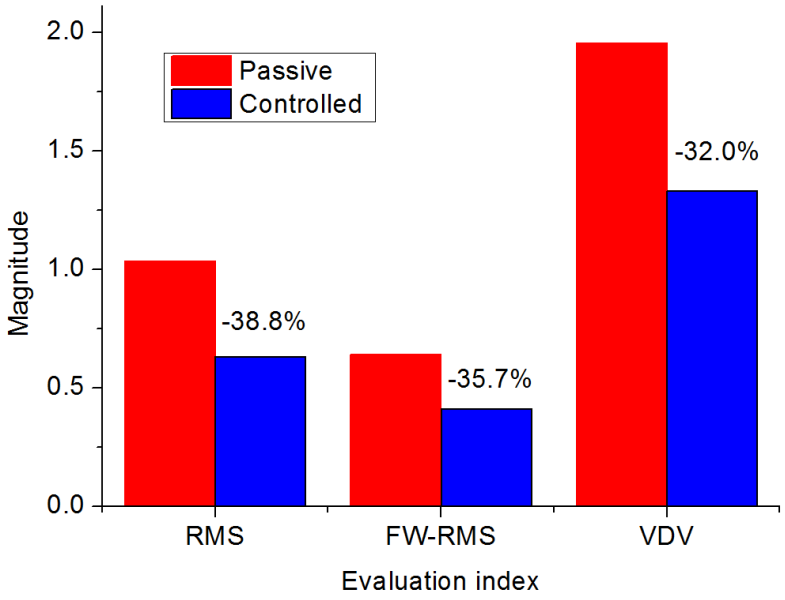

Figure 27. Vibration control performance.

6. Conclusions

This paper has proposed a VI device which consists of a transmission device, two flywheels and a VD device. The VI device prototype has been built by applying an electromagnetic VD device which has an electromagnetic motor and a variable resistance circuit. A connector and the stator of the motor work as a flywheel. The rotor of the motor and an additional flywheel work as another flywheel. The electromagnetic damping between the rotor and stator of the motor can control the equivalent inertance of the device. Tests designed for the applied electromagnetic VD device and the VI device prototype have helped to identify the unknown parameters and validate the proposed system model. The VI device has been applied to a seat suspension for improving the ride comfort of the heavy duty vehicle driver. The vibration transmissibility of the seat suspension in frequency domain analysis has shown the superior capability of the VI seat suspension in vibration isolation around the resonance frequency. Then, an implementable controller has validated the effectiveness of VI seat suspension. With the proposed controller, the measured current can track part of a desired active current in the random vibration experiments. Compared with a traditional passive seat suspension, the FW-RMS acceleration of the proposed system has a 35.7 % reduction, which implies the significant improvement in ride comfort. The system cost and complexity of the VI seat suspension are higher than the passive seat suspension, but it is much lower than the active one. On the other hand, the VI seat suspension has an excellent performance closing to the active one [43]. Therefore, the VI device would have a bright prospect in the vibration control application. In future research, the VI device design will be further optimised, including the design of the motor, and better controllers can be applied in practical application.

Acknowledgement

This research is supported by the Fundamental Research Funds for the Central Universities of China (JZ2019HGBH0198), and the Australian Research Council's Linkage Projects funding scheme (project number LP160100132).

References

[1] M.C. Smith, Synthesis of mechanical networks: the inerter, IEEE Transactions on Automatic Control, 47 (2002) 1648-1662.
[2] C.L.Z.X.N. Jiamei, W. Ruochen, Performance Analysis of Two-stage Series-connected Inerter-spring-damper Suspension Based on Half-car Model [J], Journal of Mechanical Engineering, 6 (2012) 017.
[3] Y. Hu, M.Z. Chen, Z. Shu, Passive vehicle suspensions employing inerters with multiple performance requirements, Journal of Sound and Vibration, 333 (2014) 2212-2225.
[4] I. Lazar, S. Neild, D. Wagg, Using an inerter-based device for structural vibration suppression, Earthquake Engineering & Structural Dynamics, 43 (2014) 1129-1147.
[5] T. Hashimoto, K. Fujita, M. Tsuji, I. Takewaki, Innovative base-isolated building with large mass-ratio TMD at basement for greater earthquake resilience, Future Cities and Environment, 1 (2015) 9.
[6] D. De Domenico, G. Ricciardi, Improving the dynamic performance of base-isolated structures via tuned mass damper and inerter devices: A comparative study, Structural Control and Health Monitoring, 25 (2018) e2234.
[7] D. De Domenico, G. Ricciardi, Optimal design and seismic performance of tuned mass damper inerter (TMDI) for structures with nonlinear base isolation systems, Earthquake Engineering & Structural Dynamics, 47 (2018) 2539-2560.
[8] C. Papageorgiou, N.E. Houghton, M.C. Smith, Experimental testing and analysis of inerter devices, Journal of dynamic systems, measurement, and control, 131 (2009) 011001.
[9] A. Gonzalez-Buelga, I.F. Lazar, J.Z. Jiang, S.A. Neild, D.J. Inman, Assessing the effect of nonlinearities on the performance of a tuned inerter damper, Structural Control and Health Monitoring, 24 (2017) e1879.
[10] F.-C. Wang, W.-J. Su, Impact of inerter nonlinearities on vehicle suspension control, Vehicle system dynamics, 46 (2008) 575-595.
[11] S. Swift, M.C. Smith, A. Glover, C. Papageorgiou, B. Gartner, N.E. Houghton, Design and modelling of a fluid inerter, International Journal of Control, 86 (2013) 2035-2051.
[12] D. De Domenico, P. Deastra, G. Ricciardi, N.D. Sims, D.J. Wagg, Novel fluid inerter based tuned mass dampers for optimised structural control of base-isolated buildings, Journal of the Franklin Institute, (2018).
[13] S. Sun, J. Yang, W. Li, H. Deng, H. Du, G. Alici, Development of a novel variable stiffness and damping magnetorheological fluid damper, Smart Materials and Structures, 24 (2015) 085021.
[14] P. Forte, M. Paternò, E. Rustighi, A magnetorheological fluid damper for rotor applications, International Journal of Rotating Machinery, 10 (2004) 175-182.
[15] S.K. Sharma, A. Kumar, Disturbance rejection and force-tracking controller of nonlinear lateral vibrations in passenger rail vehicle using magnetorheological fluid damper, Journal of Intelligent Material Systems and Structures, 29 (2018) 279-297.
[16] G.M. Kamath, M.K. Hurt, N.M. Wereley, Analysis and testing of Bingham plastic behavior in semi-active electrorheological fluid dampers, Smart Materials and Structures, 5 (1996) 576.

[17] S. Hong, S. Choi, Y. Choi, N. Wereley, Comparison of damping force models for an electrorheological fluid damper, International Journal of Vehicle Design, 33 (2003) 17-35.
[18] D. Ning, S. Sun, H. Du, W. Li, N. Zhang, Vibration control of an energy regenerative seat suspension with variable external resistance, Mechanical Systems and Signal Processing, 106 (2018) 94-113.
[19] D. Ning, H. Du, S. Sun, W. Li, W. Li, An energy saving variable damping seat suspension system with regeneration capability, IEEE Transactions on Industrial Electronics, (2018).
[20] Y. Liu, H. Matsuhisa, H. Utsuno, Semi-active vibration isolation system with variable stiffness and damping control, Journal of sound and vibration, 313 (2008) 16-28.
[21] H. Du, W. Li, N. Zhang, Semi-active variable stiffness vibration control of vehicle seat suspension using an MR elastomer isolator, Smart materials and structures, 20 (2011) 105003.
[22] J. Yang, H. Du, W. Li, Y. Li, J. Li, S. Sun, H. Deng, Experimental study and modeling of a novel magnetorheological elastomer isolator, Smart Materials and Structures, 22 (2013) 117001.
[23] S. Sun, H. Deng, H. Du, W. Li, J. Yang, G. Liu, G. Alici, T. Yan, A compact variable stiffness and damping shock absorber for vehicle suspension, IEEE/ASME Transactions on Mechatronics, 20 (2015) 2621-2629.
[24] M.Z. Chen, Y. Hu, C. Li, G. Chen, Performance benefits of using inerter in semiactive suspensions, IEEE Transactions on Control Systems Technology, 23 (2015) 1571-1577.
[25] Y. Hu, K. Wang, Y. Chen, M.Z. Chen, Inerter-based semi-active suspensions with low-order mechanical admittance via network synthesis, Transactions of the Institute of Measurement and Control, (2018) 0142331217744852.
[26] M. Chen, Y. Hu, C. Li, G. Chen, Semi-active suspension with semi-active inerter and semi-active damper, Proceedings of the 19th IFAC World Congress, 2014, International Federation of Automatic Control., 2014.
[27] Y. Hu, M.Z. Chen, S. Xu, Y. Liu, Semiactive inerter and its application in adaptive tuned vibration absorbers, IEEE Transactions on Control Systems Technology, 25 (2017) 294-300.
[28] D. Ning, S. Sun, J. Yu, M. Zheng, H. Du, N. Zhang, W. Li, A rotary variable admittance device and its application in vehicle seat suspension vibration control, Journal of the Franklin Institute, (2019).
[29] T.D. Le, K.K. Ahn, A vibration isolation system in low frequency excitation region using negative stiffness structure for vehicle seat, Journal of Sound and Vibration, 330 (2011) 6311-6335.
[30] Z. Gan, A.J. Hillis, J. Darling, Adaptive control of an active seat for occupant vibration reduction, Journal of Sound and Vibration, 349 (2015) 39-55.
[31] I. Maciejewski, L. Meyer, T. Krzyzynski, The vibration damping effectiveness of an active seat suspension system and its robustness to varying mass loading, Journal of Sound and Vibration, 329 (2010) 3898-3914.
[32] K.K. Ahn, Active pneumatic vibration isolation system using negative stiffness structures for a vehicle seat, Journal of Sound and Vibration, 333 (2014) 1245-1268.
[33] D. Ning, S. Sun, H. Li, H. Du, W. Li, Active control of an innovative seat suspension system with acceleration measurement based friction estimation, Journal of Sound and Vibration, 384 (2016) 28-44.
[34] S.-B. Choi, Y.-M. Han, Vibration control of electrorheological seat suspension with human-body model using sliding mode control, Journal of Sound and Vibration, 303 (2007) 391-404.
[35] S. Sun, D. Ning, J. Yang, H. Du, S. Zhang, W. Li, A seat suspension with a rotary magnetorheological damper for heavy duty vehicles, Smart Materials and Structures, 25 (2016) 105032.
[36] J.-Y. Li, S. Zhu, Versatile Behaviors of Electromagnetic Shunt Damper With a Negative Impedance Converter, IEEE/ASME Transactions on Mechatronics, 23 (2018) 1415-1424.
[37] Z. Li, L. Zuo, G. Luhrs, L. Lin, Y.-x. Qin, Electromagnetic energy-harvesting shock absorbers: design, modeling, and road tests, IEEE Transactions on Vehicular Technology, 62 (2013) 1065-1074.
[38] N. Mabbott, G. Foster, B. McPhee, Heavy vehicle seat vibration and driver fatigue, 2001.

[39] S.D. Nguyen, W. Kim, J. Park, S.-B. Choi, A new fuzzy sliding mode controller for vibration control systems using integrated-structure smart dampers, Smart Materials and Structures, 26 (2017) 045038.
[40] S.D. Nguyen, S.-B. Choi, A new neuro-fuzzy training algorithm for identifying dynamic characteristics of smart dampers, Smart Materials and Structures, 21 (2012) 085021.
[41] S.D. Nguyen, Q.H. Nguyen, S.-B. Choi, A hybrid clustering based fuzzy structure for vibration control–Part 2: An application to semi-active vehicle seat-suspension system, Mechanical Systems and Signal Processing, 56 (2015) 288-301.
[42] ISO, Mechanical Vibration and Shock – Evaluation of Human Exposure to Whole-body Vibration – Part 1: General Requirements, ISO 2631–1, (1997).
[43] D. Ning, S. Sun, J. Zhang, H. Du, W. Li, X. Wang, An active seat suspension design for vibration control of heavy-duty vehicles, Journal of low frequency noise, vibration and active control, 35 (2016) 264-278.